Synthetic Control of Retinal Photochemistry and Photophysics in Solution

Giovanni Bassolino,[†] Tina Sovdat,[‡] Matz Liebel,[†] Christoph Schnedermann,[†] Barbara Odell,[‡] Timothy D.W. Claridge,[‡] Philipp Kukura,*[,†] and Stephen P. Fletcher*[,‡]

[†]Department of Chemistry, Physical and Theoretical Chemistry Laboratory, University of Oxford, South Parks Road, Oxford OX1 3QZ, U.K.

[‡]Department of Chemistry, Chemistry Research Laboratory, University of Oxford, Mansfield Road, Oxford OX1 3TA, U.K.

Ⓢ Supporting Information

ABSTRACT: Understanding how molecular structure and environment control energy flow in molecules is a requirement for the efficient design of tailor-made photochemistry. Here, we investigate the tunability of the photochemical and photophysical properties of the retinal-protonated Schiff base chromophore in solution. Replacing the n-butylamine Schiff base normally chosen to mimic the saturated linkage found in nature by aromatic amines results in the reproduction of the opsin shift and complete suppression of all isomerization channels. Modification of retinal by directed addition or removal of backbone substituents tunes the overall photoisomerization yield from 0 to 0.55 and the excited state lifetime from 0.4 to 7 ps and activates previously inaccessible reaction channels to form 7-cis and 13-cis products. We observed a clear correlation between the presence of polarizable backbone substituents and photochemical reactivity. Structural changes that increase reaction speed were found to decrease quantum yields, and vice versa, so that excited state lifetime and efficiency are inversely correlated in contrast to the trends observed when comparing retinal photochemistry in protein and solution environments. Our results suggest a simple model where backbone modifications and Schiff base substituents control barrier heights on the excited-state potential energy surface and therefore determine speed, product distribution, and overall yield of the photochemical process.
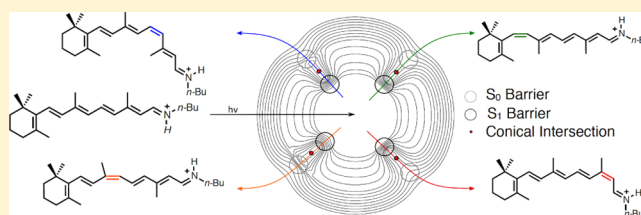
■ INTRODUCTION

The retinal chromophore is ubiquitously used in nature to transform light into chemical, mechanical, or electrical energy.[1] The desired function is invariably performed by a surrounding protein but is initiated by an efficient photoisomerization of retinal covalently bound via a protonated Schiff base linkage. Although the choice of chromophore is convenient from a metabolic perspective, its reactivity, spectral overlap with the solar emission spectrum, and photochemical specificity are poor for retinal and retinal protonated Schiff bases (RPSBs) in the absence of a protein environment.[2−5] Remarkably, all of these parameters are dramatically improved in retinal-containing proteins, which is in line with the idea of optimized photobiological function. The discrepancy between solution and protein behavior has been largely attributed to the complexity of the protein pocket with its three-dimensional arrangement of amino acids resulting in a unique steric and dielectric environment.[6,7]

The tunability of absorption spectra, isomerization yield, and reaction speed makes RPSB the ideal candidate for investigations aiming to unravel the molecular and structural origins of efficient photochemistry.[6−15] As a consequence, RPSB has become a paradigm for understanding the origins of activation and suppression of ultrafast relaxation processes, which is essential for the rational engineering of photoreactivity. Despite numerous efforts, however, the reactive properties of

RPSB in solution have been largely resistant to synthetic or environmental control. Small variations in both quantum yields (QYs) and excited state lifetimes (ESLs) have been reported,[16−20] but it has never been possible to mimic the features observed in opsin photochemistry. The differences in RPSB reactivity between solution and protein environments are most dramatically illustrated by the photochemical properties of the chromophore in the bacterial proton pump bacterioRhodopsin (bR)[21,22] and in solution[2] (Table 1). The red shift of

Table 1. Retinal Protonated Schiff Base Photochemistry in Protein and Solution

R	Lys	n-Bu
abs λ_{max} (nm)	568	446
Excited State Lifetime (ps)	0.5	4.3
Product (Quantum Yield)	13-cis(0.64)	11-cis(0.16) 9-cis (0.05)

the absorption spectrum in the protein, the so-called "opsin shift", has been investigated in detail synthetically, spectroscopically, and computationally.[4,10,23−33] The currently accepted mechanism of color tuning is that the absorption maximum is determined by the dielectric environment of the retinal binding pocket.[34−37]

Addressing other aspects of opsin photochemistry is more complex, and a widely adopted approach has been to prepare pigment analogues containing retinal derivatives with modified backbones.[8,38−42] Taken together, these studies point toward protein-induced steric and electrostatic interactions as a primary determinant in the outcome of the photoreaction.[43−47]

To the best of our knowledge, only one study on the photochemistry of a RPSB with a modified retinal backbone (11-*cis*-13-demethyl RPSB) in solution has been reported.[48] In our recent exploratory work,[49] we demonstrated that addition of a methyl group to the 10-position of the retinal backbone dramatically affects RPSB solution photochemistry, reducing the ESL by almost 1 order of magnitude from 4 to 0.55 ps toward the lifetime observed in bR (0.5 ps). Together with the changes in ESL, the modification caused a 50% decrease in the isomerization yield, suggesting an inverse correlation between reaction speed and yield, but could only provide an incomplete picture as to the mechanistic origin of the observed effect.

In this work, we systematically explored the influence of both backbone and Schiff base substitution on RPSB photochemistry. By appropriate choice of the Schiff base, we succeeded in reproducing the shift of absorption maximum observed for RPSBs in the protein environment, with the tail of the absorption reaching all the way to the near-infrared (700 nm). Addition or removal of polarizable substituents from the retinal backbone for the natural *n*-butyl (*n*Bu) protonated Schiff base allowed us to tune the ESL from 400 fs to 7 ps and achieve a spread of the overall reaction yield from effectively 0 to 0.55. We further induced changes in the selectivity of these reactions, either completely closing secondary isomerization pathways or obtaining 7-*cis* or 13-*cis* isomers rather than the 9-*cis* isomer observed with natural RPSB in solution (see the Supporting Information, Figure SF18). Our results demonstrate that remarkable tunability of RPSB photochemistry can be achieved in solution, without a specific spatial, steric, and dielectric environment as provided by a protein pocket evolved through natural selection.

■ MATERIALS AND METHODS

Synthesis. We used the general synthetic approach depicted in Scheme 1 to prepare a library of retinal derivatives (Table 2). A series of consecutive Horner−Wadsworth−Emmons (HWE) reactions and DIBAL-H reductions were employed to prepare the modified retinals
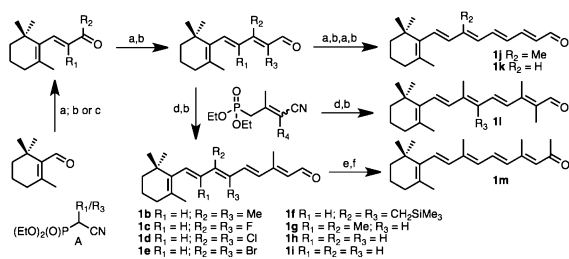
Table 2. Chain Substituents for the Backbone-Modified Retinals

Compound	X8	X9	X10	X13	X14	X15
NAT (1a)	H	Me	H	Me	H	H
10Me (1b)	H	Me	Me	Me	H	H
10F (1c)	H	Me	F	Me	H	H
10Cl (1d)	H	Me	Cl	Me	H	H
10Br (1e)	H	Me	Br	Me	H	H
10Si (1f)	H	Me	CH$_2$Si(CH$_3$)$_3$	Me	H	H
8Me (1g)	Me	Me	H	Me	H	H
9-dm (1h)	H	H	H	Me	H	H
13-dm (1i)	H	Me	H	H	H	H
9,13-dm (1j)	H	H	H	H	H	H
14Me (1k)	H	Me	H	Me	Me	H
10,14-Me (1l)	H	Me	Me	Me	Me	H
15Me (1m)	H	Me	H	Me	H	Me

(**2b−m**) (Scheme 1).[12] Substituents at C$_{10}$ of the backbone (derivatives **2b−f,l**) were introduced via coupling of commercially available β-ionone with the appropriate phosphonate **A**.[50,51] The HWE reaction inevitably generated a mixture of *E/Z*-isomers. However, subsequent reduction to the aldehyde allowed for the isolation of the desired isomer in all cases. The chain was then extended with (*E/Z*)-diethyl (3-cyano-2-methylallyl)phosphonate;[50,52,53] again generating a mixture of isomers. Upon reduction, *all-trans* C$_{10}$-substituted retinals were isolated (**2b−f**). The methyl group at position 14 of the retinal backbone (**2k,l**) was installed using a methylated modification of (*E/Z*)-diethyl (3-cyano-2-methylallyl)phosphonate[52] prepared from chloroacetone and diethyl(cyanoethyl)phosphonate. Methylation of C$_8$ (**2g**) was implemented through HWE coupling of β-cyclocitral with diethyl (cyanoethyl)phosphonate. The methyl group at C$_9$ was introduced via addition of MeLi to the resulting nitrile.[54] The polyene chain was extended in a manner analogous to the C$_{10}$-substituted retinal synthesis. Addition of a methyl group to C$_{15}$ (**2m**) was achieved through quantitative 1,2-addition of MeLi to commercially available *all-E*-retinal[55] followed by oxidation with catalytic TPAP, which was found to be a more suitable oxidizing agent than MnO$_2$ or Dess−Martin periodinane.

Demethylated retinal analogues (**2h−j**) were accessed by stepwise formation of additional double bonds from the ring toward the aldehyde functional group so that demethylation at C$_9$ (**2h**) was obtained through two consecutive cycles of HWE coupling followed by DIBAL reduction starting from β-cyclocitral. Likewise, C$_{13}$ methyl group removal (**2i**) employs an analogous strategy starting from the appropriate aldehyde.

Schiff base formation was achieved by condensing a retinal (**2a−m**) with the appropriate amine. Chromophores containing aliphatic amines were prepared by stirring the two components for 1 h at 0 °C over dry 4 Å molecular sieves in methanol under rigorously dark conditions. Imines with aromatic amine moieties were prepared at room temperature with extended reaction times (10−12 h). Formation of protonated Schiff bases (**1a−m** and **3−5**, see Figure 2) was achieved via the addition of a drop of neat trifluoroacetic acid (TFA) to a solution of the imine in methanol.[56] All photosensitive materials were handled under dim red light illumination. See the Supporting Information for details of the preparation, purification, and characterization of each derivative.

Ultrafast Spectroscopy. Laser pulses were delivered by a LightConversion PHAROS-6W amplifier (1030 nm, 180 fs, 5.5 W at 10 kHz). Fifteen milliwatts of the output was used for white light generation in sapphire to generate broadband probe pulses. The remainder was used for second-harmonic generation (SHG) in BBO followed by sum frequency generation (SFG) between second harmonic and fundamental (BBO).[57] The obtained output at 343 nm (500 mW) pumped a white-light seeded two-stage noncollinear optical parametric amplifier NOPA[58] to generate the excitation pulse (500 nm, 25 fs, 30 mW). The pump was compressed using chirped mirrors (Layertec) and characterized with SHG frequency-resolved
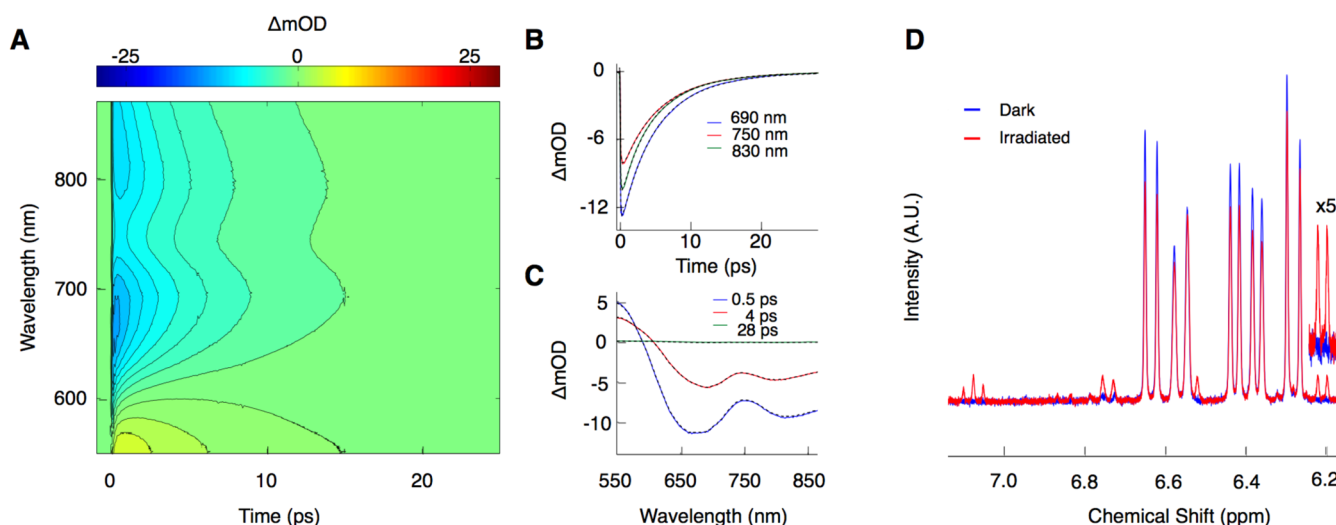
Scheme 1. Synthesis of Modified Retinal Chromophores^a

1j R$_2$ = Me
1k R$_2$ = H

1b R$_1$ = H; R$_2$ = R$_3$ = Me
1c R$_1$ = H; R$_2$ = R$_3$ = F
1d R$_1$ = H; R$_2$ = R$_3$ = Cl
1e R$_1$ = H; R$_2$ = R$_3$ = Br
1f R$_1$ = H; R$_2$ = R$_3$ = CH$_2$SiMe$_3$
1g R$_1$ = H; R$_2$ = Me; R$_3$ = H
1h R$_1$ = R$_2$ = R$_3$ = H
1l R$_1$ = R$_2$ = R$_3$ = H

^{a}Key: (a) BuLi, **A**; (b) DIBAL-H; (c) MeLi; (d) BuLi; (e) MeLi; (f) TPAP, NMO.

Figure 1. Experimental approach to determine RPSB photochemistry. (A) Differential absorbance map as a function of time delay and probe wavelength recorded for natural *n*Bu RPSB (**1a**). (B) Time traces at selected probe wavelengths throughout the stimulated emission band. (C) Transient absorption spectra corresponding to the temporal evolution of the data. (D) Typical ^{1}H NMR spectra before and after irradiation of natural *n*Bu RPSB.

optical gating (FROG)[59] in a 10 μm BBO. A flow cell with path length of 500 and 120 μm windows was used for the experiments. The flow speed was adjusted to replenish the sample between consecutive pulses. The diameters of the pump and probe beams were measured to be 150 and 50 μm, with the pulse energies adjusted to 20 and 2 nJ, respectively. Broadband detection was performed by a home-built single shot prism spectrograph[60] equipped with a LW-ELIS-1024A-1394 detector. We corrected the differential absorbance maps for probe chirp from solvent only traces to generate transient absorption traces as a function of probe wavelength and time delay (Figure 1A) and then fitted the latter via a global optimization routine.[61] All transient absorption data analysis was performed in MATLAB.[62] The dynamics of all compounds could be described by a triexponential function convolved with a Gaussian instrument response and a step function (Figure 1B). Typical transient differential absorption spectra are shown in Figure 1C. The three time constants ranged from 0.2−0.4, 0.5−3, and 3−10 ps for the first, second, and third constant, respectively (see the Supporting Information, Table S1 and Figures SF1−SF17, for details on each compound). The coherent response due to the overlap of the pump and probe pulse is modeled with a combination of Gaussian derivatives up to the ninth order.

Determining the Excited State Lifetime. The differential absorption between 550 and 850 nm was used to evaluate the average lifetime for each RPSB. From the global optimization routine, each time constant was retrieved together with a decay associated spectrum (DAS).[61] For all detection wavelengths within the stimulated emission (SE) band (~600−850 nm) the average ESL was evaluated as a weighted average of the decay constants and the absolute value of the DAS amplitude, according to the following formula:

$$\mathrm{ESL}_\lambda = \frac{\sum_k \tau_k \cdot |\mathrm{DAS}_{k\lambda}|}{\sum_k |\mathrm{DAS}_{k\lambda}|} \tag{1}$$

The values reported in the Results are the average of the lifetime values obtained along the SE band (see the Supporting Information, Table S1, for details on each compound).

Quantum Yield Measurements. A CW diode-pumped solid state laser (532 nm) was used to irradiate a glass test tube containing 1 mL of a stirred ~3 mM (OD ≫ 2) solution of RPSB in CD$_3$OD. Expanding the beam to a diameter of 0.8 cm at an incident power of 0.2 mW resulted in irradiation in the linear regime. Experiments were performed in such conditions to ensure less than 10% conversion of the starting material, so that irradiation times ranged between 15 and 40 min depending on the isomerization yield. The amount of

photoproduct formed was determined by 500 or 700 MHz ^{1}H NMR spectroscopy by integration, comparing the average of several starting material signals with the average of several product signals (Figure 1D). Sample concentration was determined by adding 10 μL of a 1% v/v solution of an appropriate internal standard to 700 μL of nonirradiated RPSB and comparing the average area of the RPSBs signals with the internal standard in the ^{1}H NMR spectrum (see the Supporting Information, Table S2, for details on the internal standards used for each compound).

For the aromatic amine containing compounds (**3−5**, Figure 2), the QY and excited state dynamics were measured in CH$_3$CN or CD$_3$CN. For this class of compounds no isomerization product was detectable via ^{1}H NMR spectroscopy.

Photoproduct Determination. Irradiations of the RPSBs were carried out as described above, adjusting the reaction time to achieve ~20% conversion. Under these conditions, no new species were formed as determined by ^{1}H NMR spectroscopy. Photoproducts were identified by 1D and/or 2D NOESY, TOCSY, and COSY experiments (see the Supporting Information).[63] In some cases, photoproducts were identified by comparison with a fully characterized synthetic standard (see the Supporting Information).

Computational Methods. Ground-state optimized geometries for all molecules studied in this paper were obtained with Gaussian 09[64] using the wb97xd/cc-pVDZ potential.[65,66] As a test for the optimized structure to be a local minimum, the second derivatives of the Hessian matrix were checked to be positive.[67] Merz−Kollman (MK) partial atomic charges[68,69] for the ground and first singlet excited state were evaluated with the wb97xd/6-31+G(d,p)[65,70,71] potential at the ground state optimized geometry. The solvent (methanol) was treated at the CPCM level.[72,73]

RESULTS

Aromatic Amines. To reproduce the "opsin shift", we used an aromatic amine to form the Schiff base, thus introducing additional electron delocalization to the RPSB system. Three compounds (**3−5**) exhibiting a broad range of photophysical behavior, in addition to natural RPSB (**1a**), are shown in Figure 2. The red shift of the absorption when using aromatic rather than aliphatic amines can be seen in the UV−vis absorption spectra (Figure 2B). It consisted of up to 90 nm (to 534 nm) for *p*-phenylenediamine RPSB **5** relative to *n*Bu RPSB **1a**. In addition, the spectra broadened considerably. In contrast to the uniform trend observed for shifts in the absorption maximum,
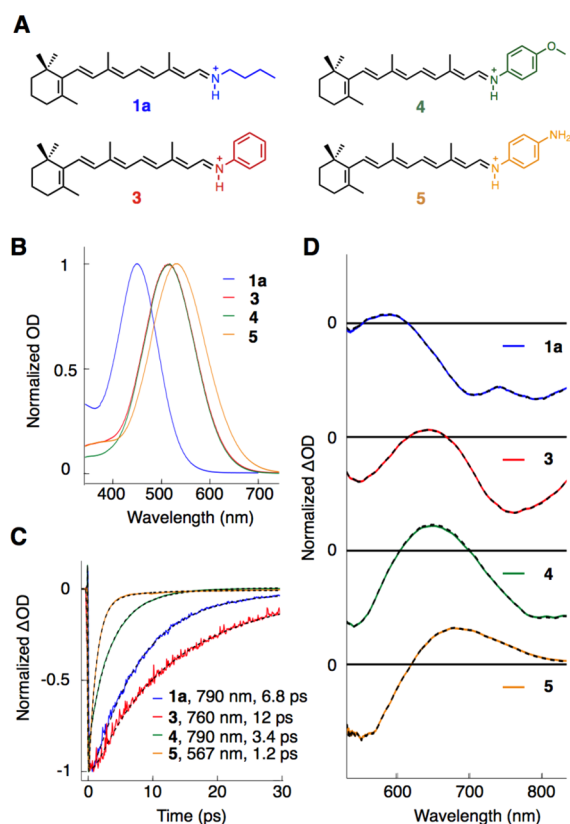
Figure 2. Modification of the Schiff base. Comparison for RPSBs obtained with aromatic amines (A) structures, (B) absorption spectra, (C) decay kinetics, and (D) transient spectra at 1 ps after photoexcitation with a resonant 25 fs pump pulse. Dashed lines represent the fits obtained from the global optimization routine.

the effect of the extended π-system on the ESLs (Figure 2C) differed: In two cases, p-methoxyaniline RPSB (**4**) and p-phenylenediamine RPSB (**5**), the lifetime decreased compared to natural RPSB (**1a**) (3.4 and 1.2 ps vs 6.8 ps, respectively), while in the case of the unsubstituted aniline (**3**) it increased (12 ps).

A comparison of the transient spectra at 1 ps delay time for natural nBu RPSB (**1a**) and the three aromatic derivatives (**3**–**5**) is shown in Figure 2D. The features of the transient spectrum of natural nBu RPSB (**1a**) are well-known including a broad SE band (600→900 nm) overlapping with an excited-state absorption band (ESA) that results in a distinctive double peak shape. Another ESA band is present at 580 nm, with the tail of the ground-state bleach (GSB) visible up to 550 nm.[74] The most striking feature for the aromatic derivatives (**3**–**5**) is the separation and reduced spectral overlap of the red ESA and SE bands. As the absorption maxima for these derivatives is considerably red-shifted, the GSB is now clearly visible in our observation window up to ~600 nm. Remarkably, the isomerization yield for all RPSBs with aromatic Schiff bases (**3**–**5**) is zero.

Modification of the Retinal Backbone. While extending the π-system allowed us to reproduce the "opsin shift", it did not enable us to change the topography of the excited-state potential energy surface (PES) and change the QY beyond completely halting photoisomerization. Prompted by published work reporting a considerable electron redistribution following excitation for RPSBs,[75,76] we evaluated the difference in MK partial atomic charges between the first excited singlet state and

the ground electronic state for natural nBu RPSB (**1a**) (Figure 3). A positive sign of this charge difference corresponds to
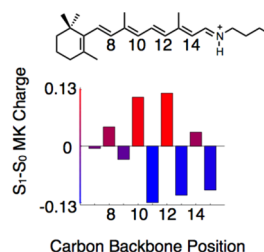

Figure 3. Difference in MK charges of the excited and ground states for polyene chain carbons of natural nBu RPSB **1a**.

depletion of electron density, while a negative sign to an increase in electron density for the atom in question. One would thus expect the effect of backbone substitution to be greatest on the topography of the excited electronic state when there is a significant difference in electron density upon excitation. Based on this reasoning, we focused on two types of synthetic modifications: addition or removal of methyl groups from the natural backbone (**2b** and **g**–**m**), and addition of substituents with different electronic character at the C10 position (**2b**–**f**). The former class of compounds allowed us to probe the effect of the substitution position, while the latter helped us to understand the importance of the character of the substitution. Evaluation of the ground state MK partial atomic charges and the difference in MK charges upon excitation revealed a pattern for these new derivatives qualitatively similar to the one found for natural RPSB (**1a**), but differences were observed at the position of substitution (see the Supporting Information, Figures SF19–21).

The results of the photochemical investigation on the examined compounds are reported in Figure 4. A general trend for the effects of substitution on the photochemistry becomes immediately clear: all derivatives with substituents added to the backbone (**1b**–**g** and **1k**–**m**) exhibit faster excited state decay than natural nBu RPSB **1a**, while demethylation (**11h**–**j**) increases the ESL. The only exception is 9-demethyl RPSB **1h**, which exhibits a slightly lower ESL than **1a**. The ESL can be tuned over a range of values smaller than for the chromophore in bacterioRhodopsin (500 fs), as in the case of 10,14-dimethyl RPSB **1l** (400 fs), to more than 1 order of magnitude larger than in bR, in the case of 9,13-demethyl **1j** (7 ps). Addition of substituents at the 10-position always shortens the ESL, and the effect is correlated with the polarizability of halogenated substituents (Br > Cl > F). A single demethylation (**1i**) extends the ESL, with removal of both methyl backbone groups (**1j**) having the largest effect in this sense.

A similar trend is observed for the corresponding QY of isomerization (Figure 4B). Removal of backbone substituents (**1h**–**j**) increases the total isomerization yield, while the addition of substituents (**1b**–**g** and **1k**–**m**) reduces the yield. The tunability ranges from a barely detectable overall yield (≪0.02) for 10-chloro RPSB **1d** to a total yield of 0.55 for the 13-demethyl isomer (**1i**). For those species where the photoproducts identities could be determined, the major photoproduct was the 11-*cis* isomer. Addition or removal of substituents in the 9- and 10-position (**1b,c,f**) led to an increased reaction selectivity, with yields as high as 25% in the case of the 9-demethyl RPSB (**1h**). In contrast, addition of methyl-groups to other C═C bonds (**1g,k,m**) activated
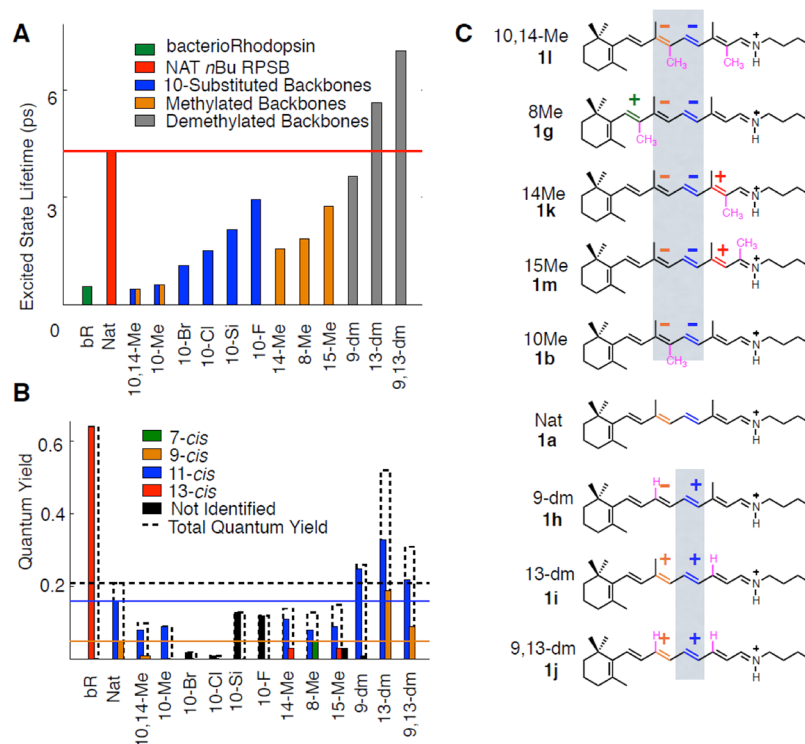
Figure 4. Kinetics and isomerization yields for backbone-modified RPSB derivatives in solution. (A) Excited state lifetimes and (B) QY for photoproduct formation. The values for bR are taken from refs 21 and 22. (C) Structures of the (de)methylated *all-trans* isomers and changes to isomerization yields. Backbone modifications are shown in pink. Isomerizing bonds are colored according to the graph in B. "+" or "−" signs refer to the change in quantum yield for the corresponding double bond with respect to **1a**.

isomerization channels previously silent in the natural backbone **1a**. Most notably, these included the activation of the 7,8 C=C isomerization upon methylation of the 8-position (**1g**), and the activation of the 13,14 C=C channel upon methylation of the 14- and 15- positions (**1k** and **1m**, respectively). The latter is the only channel active in the isomerization of retinal in the bacteriorhodopsin proton pump, and this photoisomerization channel is undetectable in our measurements of natural *n*Bu RPSB after prolonged irradiation (**1a**) (see the Supporting Information, Figure SF18). The changes in isomerization yield, illustrated as '+' for increasing or opening a photoisomerization channel, and '−' for decreasing or closing a pathway upon (de)methylation of the backbone, are summarized in Figure 4C.

DISCUSSION

Aromatic Amines. Extension of the RPSB π-system by addition of an aromatic unit as the amine moiety (**3−5**) has two major effects on the absorption spectra, red-shifting the absorption maximum by about 80 nm and allowing for limited tunability of the latter in the 520 nm region. This bathochromic shift is accompanied by changes in the ESL with no apparent trend. The presence of electron-donating groups (**4**, **5**) reduces the ESL, while it increases in their absence (**3**) with respect to natural RPSB (**1a**). Independent of the effect on the ESL, all aromatic Schiff bases are completely unreactive.

To understand the origin of the complete lack of photochemical activity, it is useful to consider the change in the distribution of the positive charge upon excitation from the ground state to the first excited singlet state.[75,76] For the natural *n*Bu RPSB, a partial translocation of the positive charge is observed predominantly toward the β-ionone ring increasing

the single bond character of C=C bonds, and vice versa. This dramatic change in equilibrium bond lengths upon excitation is well reflected in the ground-state preresonance Raman spectra of RPSB that are dominated by C−C and C=C stretching coordinates,[77] as expected for strongly displaced modes (Figure 5A).[78] Replacing the *n*Bu moiety with an aromatic one has only a negligible effect on the appearance of the Raman spectrum, except for a splitting of the C=C stretching band (1500 cm^{-1} region) caused by symmetric and asymmetric combination of the backbone stretching with the Schiff base stretching modes (Figure 5A). Calculations of the MK charges for the optimized ground-state geometry (Figure 5B) and charge differences at the same point between first excited state and ground state (Figure 5C) show remarkable similarity independent of the Schiff base character.

These observations suggest that the nature of the excited electronic state in the Franck−Condon region, the character of the initial charge translocation, and the resulting changes in bond lengths are very similar irrespective of the nature of the Schiff base. The dramatic suppression of photochemical reactivity must therefore have its origin outside the Franck−Condon region. A possibility is that the addition of the aromatic amine not only serves to extend the π-system but also to provide an alternative relaxation channel such as a twisted intramolecular charge transfer (TICT)[79] state, from which the system can decay efficiently without backbone isomerization.

An alternative, but useful, interpretation focuses on the conversion of photon into nuclear kinetic energy in the form of vibrational excitations. The latter are critical in determining the rate constants for the various relaxation channels and thus branching ratios for ultrafast decay processes that take place on time scales faster or comparable to vibrational relaxation times.
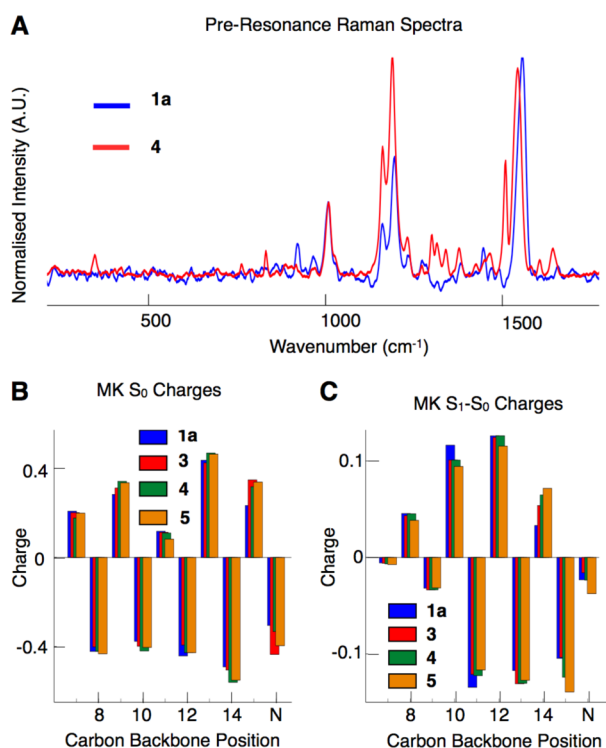
Figure 5. Electronic character in the Franck−Condon region is unchanged upon substitution of an aromatic Schiff base. (A) Preresonance Raman spectra of natural *n*Bu RPSB (**1a**) and *p*-methoxyaniline RPSB (**4**). (B) MK charges for the ground electronic state. (C) Difference in MK charges between ground and first excited state computed for different protonated Schiff bases.

Charge translocation necessarily causes dramatic changes in equilibrium bond lengths, which in turn causes the deposition of photon energy in nuclear coordinates that are structurally coupled to the movement of the charge. Our results suggest that the direction of energy flow is critical in determining the photochemical reactivity of retinal. If that energy flow can be influenced by electrostatic effects, charged amino acid residues

in the protein pocket could play a similar role to the aromatic amines used in this work. However, in the protein the effect is likely opposite, pushing the charge even more toward the retinal backbone compared to a simple alkane as in natural *n*Bu RPSB (**1a**). We attempted to test this hypothesis by preparing RPSBs using amines with electron-withdrawing character. Imine formation using aromatic amines bearing strongly electron-withdrawing groups proved difficult under a variety of reaction conditions. We found that imine formation was incomplete, and the products were susceptible to hydrolysis. Attempts to prepare these compounds are ongoing and provide exciting prospects for future work. Overall, controlling the direction of charge translocation and thus nuclear energy flow is a potential control mechanism for photochemical processes.

Backbone Modification. Although Schiff base modification allowed us to completely halt the photoisomerization of RPSB in solution, we could not investigate the molecular origin of photochemical reactivity and selectivity. Photoisomerization of natural all-*trans* *n*Bu RPSB (**1a**) in solution produces a mixture of 11-*cis* and 9-*cis* RPSBs, with the former being dominant. In contrast, the same process in bR produces exclusively the 13-*cis* isomer with a 3-fold higher overall yield. Comparison of parts A and B of Figure 4 shows a clear correlation between ESL and isomerization yield. In contrast to the impression created from the comparison of RPSB dynamics in proteins (bR) and in solution, which suggests that reaction speed is a prerequisite for efficient photochemistry, these results clearly demonstrate an opposite trend.

In addition, the observed specific activation and deactivation of isomerization channels depended on the position of backbone substitutions. Within the range of species studied here, we observed a wide variety of selectivity profiles and have induced isomerization for all backbone C=C double bonds. In some cases, we observed almost complete specificity (for example, 10-methyl RPSB (**1b**) and 9-demethyl RPSB (**1h**)); in other cases, the overall quantum yield approaches that observed in the bR protein environment (0.55 for **1i** vs 0.65 for bR). The observed trends qualitatively agree with a simple model based on polarizability, charge stabilization, and concomitant effects
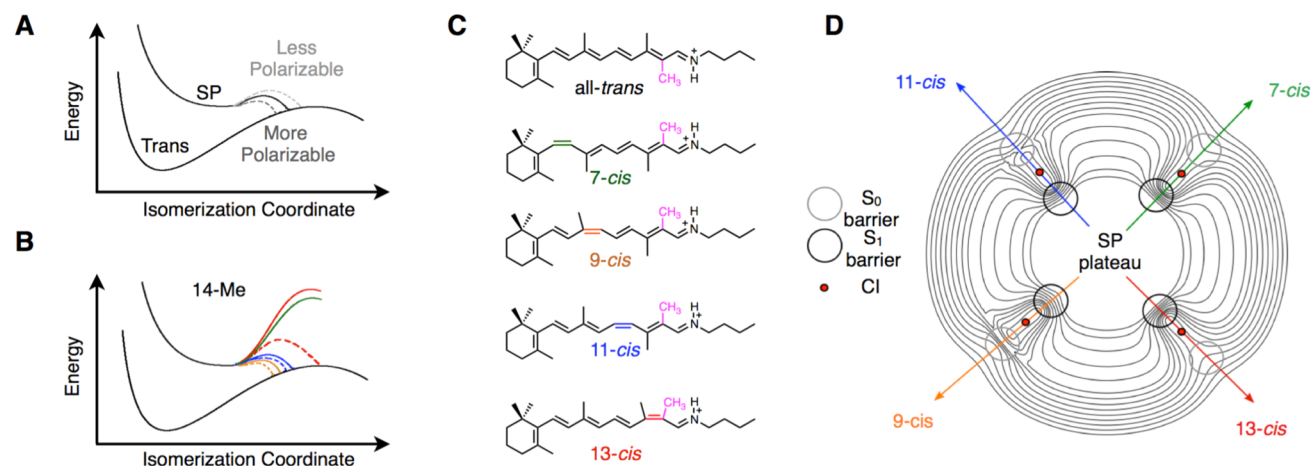

Figure 6. Modification of excited-state barrier heights as a mechanism for tuning RPSB photochemistry. (A) General effect on the addition of polarizable groups to the retinal backbone on excited-state barriers and location of the surface crossing. (B) Effect of adding a methyl group to the 14-position on the barriers toward excited-state decay using distortions toward the 7,9,11,13-cis products (green, orange, blue and red, respectively). (C). Structure for all-*trans* 14-methyl RPSB (**1k**) and the possible photoproducts. The isomerizing bonds are colored. (D) Multidimensional representation of the excited-state PES indicating all major decay pathways with differing barrier heights. SP: Stationary Point; CI: Conical Intersection.

on barrier heights resulting in different branching ratios (Figure 6).

The general trend in ESL suggests a simplified potential energy surface as shown in Figure 6A: addition of polarizable groups decreases the ESL and vice versa. The effects of change in substituent polarizability are shown as dashed lines, using solid lines to qualitatively depict the situation in natural *n*Bu RPSB (**1a**). Given that the lifetime is likely controlled by a barrier in the excited electronic state toward internal conversion,[2,15,19,80−83] it is reasonable to assume that the effect of the polarizable substituents is to lower that barrier. The correlation between ESL and isomerization yield suggests this to be a consequence of the barrier lowering. This observation is in line with isomerization coordinates at least partially contributing to excited state decay and a lower barrier leading to an earlier crossing along the isomerization coordinate, which in turn results in lower isomerization yield. Such early crossing agrees with experiments on bacteriorhodopsin that showed how the initial stationary point reached in the excited electronic state, after relaxation out of the Franck−Condon region, corresponds to only a little evolution along the isomerization coordinate.[84] Additional support for this hypothesis has been recently provided by high-level quantum chemical calculations that observed the existence of a barrier on the excited electronic state on the path toward the conical intersection (CI).[15,83] Furthermore, the connection between internal conversion and isomerization coordinate is in agreement with the symmetries of any vibrational modes coupling the two electronic states of different symmetry, i.e., a requirement for nontotally symmetric modes, such as backbone torsions and hydrogen wags. Models that involve excited-state decay by distortion of the backbone require that, at least in principle, all C=C bonds can mediate internal conversion and thus appear as potential photoproducts. The product distribution would then depend on the relative barrier heights and crossing points and could therefore be altered from the naturally occurring pathways (9-*cis* and 11-*cis*) by changing the barrier heights by backbone substitution.

As an example, consider 14-methyl RPSB (**1k**), a substitution that results in the complete suppression of the 9-*cis* channel, reduction of 11-*cis* yield, and activation of the 13-*cis* channel (Figure 6B). All of these observations are in line with the simple model introduced above. Methylation in general causes all barriers to drop, lowering the quantum yields of the naturally occurring channels (Figure 6A). In the case of 14-methyl RPSB (**1k**), 9-*cis* as a product becomes undetectable (yellow, Figure 6B), while the 11-*cis* yield drops from 0.16 to 0.11 (blue). For both the 9-*cis* and the 11-*cis* channels, the lowering of the excited state barrier leads to faster decay, but a lower yield as the surface crossing occurs earlier along the isomerization coordinate. At the same time, the 13-*cis* channel is activated (QY of 0.03) as a result of lowering of the barrier along the 13-*cis* isomerization channel sufficiently to generate a detectable amount of photoproduct (red channel). The $C_7=C_8$ double bond, however, being too distant from the point of substitution, experiences only negligible changes to the excited state barrier height, remaining inactive. We remark that exactly the same line of argument can be used to rationalize all changes in QYs observed in this work. 8-Methyl RPSB (**1g**), for example, acts in the same way as 14-methyl RPSB (**1k**), except that now the nearby $C_7=C_8$ double bond is activated while the 9-*cis* product becomes undetectable and 11-*cis* drops. Removal of methyl groups, instead, raises the barriers for all inactive channels to such a degree that they remain inactive, while a higher barrier,

even though reducing the competitivity of the channel, leads to a later CI which increases the quantum yield for the naturally active pathways (9-*cis* and 11-*cis*).

To visualize such a highly dimensional PES, it is convenient to project the individual isomerization coordinates onto nonorthogonal dimensions (Figure 6C,D). These coordinates do not represent normal modes of the molecules but simply the definition of the PES in degrees of freedom related to a backbone isomerization. Although it may appear counter-intuitive, in this representation, the system evolves along all coordinates simultaneously from the stationary point without requiring a bifurcation of the potential energy surface near the Franck−Condon region. Taken together, all of these evolutions represent the overall structural change taking place during possible isomerization reactions, as opposed to the more common backbone stretching or torsional degrees of freedom. At this stage, the barrier heights determine the possible decay rates as well as the likelihood of isomerization through the location of the crossing point as discussed for 14-methyl case (**1k**) above (Figure 6B).

Although such a model suggests multiexponential decay with component amplitudes related to the isomerization yield for each particular decay channel, their experimental observation by transient absorption spectroscopy is likely to be challenging. Although in principle additional, lower amplitude components could be added, features such as vibrational cooling make the quantification of more than three decay constants challenging as addition of more parameters tends to improve the fit so that determining a clear cut-off point is difficult. Further testing of the proposed model would thus require time-resolved vibrational spectroscopy with high sensitivity, where the growth of individual photoproducts can be observed and differentiated.

A conceptually simple, but challenging (in terms of thermal stability of the RPSB), method to obtaining high QY would be to incorporate a strongly electron-withdrawing Schiff base that pushes the charge toward the retinal backbone maximizing the activation of backbone-twisting decay channels and thus the isomerization yield. Combining such efforts with backbone modifications such as a 9-demethyl or 10-demethyl RPSB (**1h,b**, respectively) that show remarkable selectivity provides scope for the artificial design of materials with high isomerization yields and specificity to an extent that was thought to exist only in an evolution-optimized, three-dimensional protein environment.

The correlation between ESL, QY, and substituent polarizability suggests an electronic origin of the excited-state barrier. As noted by others[85] numerous polarizable aromatic residues are present in the protein pocket and recent spectroscopic[37] and computational[36] studies have described color tuning by modulation of the electrostatic environment. Our results demonstrate that it is possible to control the yield, speed and selectivity by addition or removal of polarizable groups along the backbone, or appropriate choice of the amine for Schiff base formation. In the case of bR and opsin proteins, which exhibit exquisite control over all of these factors, it remains unclear how to reproduce the degree of selectivity observed in nature — but our results point toward a mechanism in which nonbonded interactions between the retinal chromophore and amino acid residues in the protein pocket can be used to provide complete control of retinal photochemistry. Testing the validity of this hypothesis and unraveling the details of these isomerization mechanisms offers considerable prospects for future work and our eventual understanding of these processes.

CONCLUSIONS

Our overall model of charge stabilization, either by the Schiff base or by addition of polarizable groups to the backbone, suggests a simple but powerful mechanism that allows tuning of photochemical reactivity by rational, synthetic design. The general methodology of synthetic tuning and spectroscopic characterization was applied to retinal isomerization due to the extensive experimental and theoretical literature precedent. Applications to energy or electron transfer for other chromophores found in evolution optimized protein environments will be equally possible in the future.

ASSOCIATED CONTENT

Ⓢ Supporting Information

Synthetic procedure and characterization data for all compounds and details of the analysis on the transient absorption data, QY measurement, and MK charge analysis. This material is available free of charge via the Internet at http://pubs.acs.org

AUTHOR INFORMATION

Corresponding Authors

philipp.kukura@chem.ox.ac.uk
stephen.fletcher@chem.ox.ac.uk

Notes

The authors declare no competing financial interest.

ACKNOWLEDGMENTS

REFERENCES

(1) Spudich, J.; Yang, C.; Jung, K.; Spudich, E. *Annu. Rev. Cell Dev. Biol.* **2000**, *16*, 365.
(2) Freedman, K. A.; Becker, R. S. *J. Am. Chem. Soc.* **1986**, *108*, 1245.
(3) Waddell, W. H.; Crouch, R.; Nakanishi, K.; Turro, N. J. *J. Am. Chem. Soc.* **1976**, *98*, 4189.
(4) Blatz, P. E.; Liebman, P. A. *Exp. Eye Res.* **1973**, *17*, 573.
(5) Fukada, Y.; Okano, T.; Shichida, Y.; Yoshizawa, T.; Trehan, A.; Mead, D.; Denny, M.; Asato, A. E.; Liu, R. S. H. *Biochemistry* **1990**, *29*, 3133.
(6) Kochendoerfer, G.; Lin, S.; Sakmar, T.; Mathies, R. *Trends Biochem. Sci.* **1999**, *24*, 300.
(7) Verhoeven, M.; Bovee-Geurts, P.; de Groot, H.; Lugtenburg, J.; DeGrip, W. *J. Mol. Biol.* **2006**, *363*, 98.
(8) Ottolenghi, M.; Sheves, M. *J. Membr. Biol.* **1989**, *112*, 193.
(9) Becker, R. S. *Photochem. Photobiol.* **1988**, *48*, 369.
(10) Wanko, M.; Hoffmann, M.; Strodel, P.; Koslowski, A.; Thiel, W.; Neese, F.; Frauenheim, T.; Elstner, M. *J. Phys. Chem. B* **2005**, *109*, 3606.
(11) Mathies, R.; Lin, S.; Ames, J.; Pollard, W. *Annu. Rev. Biophys. Biophys. Chem.* **1991**, *20*, 491.
(12) Dawadi, P.; Lugtenburg, J. *Molecules* **2010**, *15*, 1825.
(13) Altoe, P.; Cembran, A.; Olivucci, M.; Garavelli, M. *Proc. Natl. Acad. Sci. U.S.A.* **2010**, *107*, 20172.
(14) Warshel, A. *Nature* **1976**, *260*, 679.
(15) Valsson, O.; Filippi, C. *J. Chem. Theory Comput.* **2010**, *6*, 1275.
(16) Waddell, W. H.; Hopkins, D. L.; Uemura, M.; West, J. L. *J. Am. Chem. Soc.* **1978**, *100*, 1970.
(17) Waddell, W. H.; West, J. L. *J. Phys. Chem.* **1980**, *84*, 134.
(18) Blatz, P. E.; Mohler, J. H.; Navangul, H. V. *Biochemistry* **1972**, *11*, 848.
(19) Zgrablic, G.; Voitchovsky, K.; Kindermann, M.; Haacke, S.; Chergui, M. *Biophys. J.* **2005**, *88*, 2779.
(20) Bismuth, O.; Friedman, N.; Sheves, M.; Ruhman, S. *J. Phys. Chem. B* **2007**, *111*, 2327.
(21) Mathies, R. A.; Brito Cruz, C. H.; Pollard, W. T.; Shank, C. V. *Science* **1988**, *240*, 777.
(22) Tittor, J.; Oesterhelt, D. *FEBS Lett.* **1990**, *263*, 269.
(23) Yan, B.; Spudich, J. L.; Mazur, P.; Vunnam, S.; Derguini, F.; Nakanishi, K. *J. Biol. Chem.* **1995**, *270*, 29668.
(24) Sheves, M.; Kohne, B.; Mazur, Y. *J. Chem. Soc., Chem. Commun.* **1983**, 1232.
(25) Houjou, H.; Inoue, Y.; Sakurai, M. *J. Phys. Chem. B* **2001**, *105*, 867.
(26) Baloghnair, V.; Carriker, J. D.; Honig, B.; Kamat, V.; Motto, M. G.; Nakanishi, K.; Sen, R.; Sheves, M.; Tanis, M. A.; Tsujimoto, K. *Photochem. Photobiol.* **1981**, *33*, 483.
(27) Kakitani, H.; Kakitani, T.; Rodman, H.; Honig, B. *Photochem. Photobiol.* **1985**, *41*, 471.
(28) Sakmar, T. P.; Franke, R. R.; Khorana, H. G. *Proc. Natl. Acad. Sci. U.S.A.* **1991**, *88*, 3079.
(29) Neitz, M.; Neitz, J.; Jacobs, G. H. *Science* **1991**, *252*, 971.
(30) Chan, T.; Lee, M.; Sakmar, T. P. *J. Biol. Chem.* **1992**, *267*, 9478.
(31) Rajput, J.; Rahbek, D.; Andersen, L.; Hirshfeld, A.; Sheves, M.; Altoe, P.; Orlandi, G.; Garavelli, M. *Angew. Chem., Int. Ed.* **2010**, *49*, 1790.
(32) Sekharan, S.; Sugihara, M.; Buss, V. *Angew. Chem., Int. Ed.* **2007**, *46*, 269.
(33) Rajamani, R.; Lin, Y.; Gao, J. *J. Comput. Chem.* **2011**, *32*, 854.
(34) Wanko, M.; Hoffmann, M.; Frauenheim, T.; Elstner, M. *J. Phys. Chem. B* **2008**, *112*, 11462.
(35) Sudo, Y.; Yuasa, Y.; Shibata, J.; Suzuki, D.; Homma, M. *J. Biol. Chem.* **2011**, *286*, 11328.
(36) Melaccio, F.; Ferre, N.; Olivucci, M. *Phys. Chem. Chem. Phys.* **2012**, *14*, 12485.
(37) Wang, W.; Nossoni, Z.; Berbasova, T.; Watson, C.; Yapici, I.; Lee, K.; Vasileiou, C.; Geiger, J.; Borhan, B. *Science* **2012**, *338*, 1340.
(38) Corson, D.; Crouch, R. *Photochem. Photobiol.* **1996**, *63*, 595.
(39) Baasov, T.; Sheves, M. *J. Am. Chem. Soc.* **1985**, *107*, 7524.
(40) Drachev, L. A.; Drachev, A. L.; Chekulaeva, L. N.; Evstigneeva, R. P.; Kaulen, A. D.; Khitrina, L. V.; Khodonov, A. A.; Lazarova, Z. R.; Mitsner, B. I. *Arch. Biochem. Biophys.* **1989**, *270*, 184.
(41) Liu, R. S. H.; Asato, A. E. In *Chemistry and Biology of Synthetic Retinoids*; Dawson, M. I., Okamura, W. H., Eds.; CRC Press: Boca Raton, 1990; pp 51−75.
(42) Balogh-Nair, V.; Nakanishi, K. In *Chemistry and Biology of Synthetic Retinoids*; Dawson, M. I., Okamura, W. H., Eds.; CRC Press: Boca Raton, 1990; pp 147−176.
(43) Schiffmiller, R.; Callender, R. H.; Waddell, W. H.; Govindjee, R.; Ebrey, T. G.; Kakitani, H.; Honig, B.; Nakanishi, K. *Photochem. Photobiol.* **1985**, *41*, 563.
(44) deGrip, W.; deLange, F.; Bovee, P.; Verdegem, P.; Lugtenburg, J. *Pure Appl. Chem.* **1997**, *69*, 2091.
(45) Derguini, F.; Nakanishi, K. *Photobiochem. Photobiophys.* **1986**, *13*, 259.
(46) Sheves, M.; Ottolenghi, M. In *Chemistry and Biology of Synthetic Retinoids*; Dawson, M. I., Okamura, W. H., Eds.; CRC Press: Boca Raton, 1990; pp 99−123.
(47) Crouch, R. K. In *Chemistry and Biology of Synthetic Retinoids*; Dawson, M. I., Okamura, W. H., Eds.; CRC Press: Boca Raton, 1990; pp 125−146.
(48) Becker, R. S.; Freedman, K. *J. Am. Chem. Soc.* **1985**, *107*, 1477.
(49) Sovdat, T.; Bassolino, G.; Liebel, M.; Schnedermann, C.; Fletcher, S. P.; Kukura, P. *J. Am. Chem. Soc.* **2012**, *134*, 8318.

(50) DeLange, F.; Bovee-Geurts, P.; VanOostrum, J.; Portier, M.; Verdegem, P.; Lugtenburg, J.; DeGrip, W. *Biochemistry* **1998**, *37*, 1411.

(51) Iorga, B.; Ricard, L.; Savignac, P. *J. Chem. Soc., Perkin Trans. 1* **2000**, 3311.

(52) Creemers, A.; Lugtenburg, J. *J. Am. Chem. Soc.* **2002**, *124*, 6324.

(53) Trehan, A.; Mirzadegan, T.; Liu, R. S. H. *Tetrahedron* **1990**, *46*, 3769.

(54) Barakat, A.; Brenna, E.; Fuganti, C.; Serra, S. *Tetrahedron: Asymmetry* **2008**, *19*, 2316.

(55) Arens, J. F.; Van Dorp, D. A. *Nature* **1946**, *158*, 622.

(56) Delera, A. R.; Torrado, A.; Iglesias, B.; Lopez, S. *Tetrahedron Lett.* **1992**, *33*, 6205.

(57) Homann, C.; Schriever, C.; Baum, P.; Riedle, E. *Opt. Express* **2008**, *16*, 5746.

(58) Cerullo, G.; De Silvestri, S. *Rev. Sci. Instrum.* **2003**, *74*, 1.

(59) Kane, D. J.; Trebino, R. *IEEE J. Quantum Electron.* **1993**, *29*, 571.

(60) Megerle, U.; Pugliesi, I.; Schriever, C.; Sailer, C. F.; Riedle, E. *Appl. Phys. B: Lasers Opt.* **2009**, *96*, 215.

(61) Shrager, R.; Hendler, R. *J. Phys. Chem. B* **2003**, *107*, 1708.

(62) The Mathworks, Inc.: Natick, MA, 2012.

(63) Claridge, T. D. W. *High-Resolution NMR Techniques in Organic Chemistry*, 2nd ed.; Elsevier Science: Oxford, 2008.

(64) Gaussian 09, Revision A.02: Frisch, M. J.; Trucks, G. W.; Schlegel, H. B.; Scuseria, G. E.; Robb, M. A.; Cheeseman, J. R.; Scalmani, G.; Barone, V.; Mennucci, B.; Petersson, G. A.; Nakatsuji, H.; Caricato, M.; Li, X.; Hratchian, H. P.; Izmaylov, A. F.; Bloino, J.; Zheng, G.; Sonnenberg, J. L.; Hada, M.; Ehara, M.; Toyota, K.; Fukuda, R.; Hasegawa, J.; Ishida, M.; Nakajima, T.; Honda, Y.; Kitao, O.; Nakai, H.; Vreven, T.; Montgomery, J. A., Jr.; Peralta, J. E.; Ogliaro, F.; Bearpark, M.; Heyd, J. J.; Brothers, E.; Kudin, K. N.; Staroverov, V. N.; Kobayashi, R.; Normand, J.; Raghavachari, K.; Rendell, A.; Burant, J. C.; Iyengar, S. S.; Tomasi, J.; Cossi, M.; Rega, N.; Millam, N. J.; Klene, M.; Knox, J. E.; Cross, J. B.; Bakken, V.; Adamo, C.; Jaramillo, J.; Gomperts, R.; Stratmann, R. E.; Yazyev, O.; Austin, A. J.; Cammi, R.; Pomelli, C.; Ochterski, J. W.; Martin, R. L.; Morokuma, K.; Zakrzewski, V. G.; Voth, G. A.; Salvador, P.; Dannenberg, J. J.; Dapprich, S.; Daniels, A. D.; Farkas, Ö.; Foresman, J. B.; Ortiz, J. V.; Cioslowski, J.; Fox, D. J. Gaussian, Inc.: Wallingford, CT, 2009.

(65) Chai, J.; Head-Gordon, M. *Phys. Chem. Chem. Phys.* **2008**, *10*, 6615.

(66) Dunning, T. H. *J. Chem. Phys.* **1989**, *90*, 1007.

(67) Schlegel, H. B. *Wiley Interdisc. Rev.: Comput. Mol. Sci.* **2011**, *1*, 790.

(68) Singh, U. C.; Kollman, P. A. *J. Comput. Chem.* **1984**, *5*, 129.

(69) Besler, B. H.; Merz, K. M.; Kollman, P. A. *J. Comput. Chem.* **1990**, *11*, 431.

(70) Petersson, G. A.; Bennett, A.; Tensfeldt, T. G.; Allaham, M. A.; Shirley, W. A.; Mantzaris, J. *J. Chem. Phys.* **1988**, *89*, 2193.

(71) Petersson, G. A.; Allaham, M. A. *J. Chem. Phys.* **1991**, *94*, 6081.

(72) Cossi, M.; Rega, N.; Scalmani, G.; Barone, V. *J. Comput. Chem.* **2003**, *24*, 669.

(73) Barone, V.; Cossi, M. *J. Phys. Chem. A* **1998**, *102*, 1995.

(74) Bismuth, O.; Friedman, N.; Sheves, M.; Ruhman, S. *Chem. Phys.* **2007**, *341*, 267.

(75) Mathies, R.; Stryer, L. *Proc. Natl. Acad. Sci. U.S.A.* **1976**, *73*, 2169.

(76) Gonzalez-Luque, R.; Garavelli, M.; Bernardi, F.; Merchan, M.; Robb, M.; Olivucci, M. *Proc. Natl. Acad. Sci. U.S.A.* **2000**, *97*, 9379.

(77) Smith, S. O.; Myers, A. B.; Mathies, R. A.; Pardoen, J. A.; Winkel, C.; van den Berg, E. M.; Lugtenburg, J. *Biophys. J.* **1985**, *47*, 653.

(78) Lee, S. Y.; Heller, E. J. *J. Chem. Phys.* **1979**, *71*, 4777.

(79) Grabowski, Z.; Rotkiewicz, K.; Rettig, W. *Chem. Rev.* **2003**, *103*, 3899.

(80) Du, M.; Fleming, G. R. *Biophys. Chem.* **1993**, *48*, 101.

(81) Haran, G.; Wynne, K.; Xie, A.; He, Q.; Chance, M.; Hochstrasser, R. *Chem. Phys. Lett.* **1996**, *261*, 389.

(82) Kandori, H.; Sasabe, H. *Chem. Phys. Lett.* **1993**, *216*, 126.

(83) Gozem, S.; Melaccio, F.; Lindh, R.; Krylov, A. I.; Granovsky, A. A.; Angeli, C.; Olivucci, M. *J. Chem. Theory Comput.* **2013**, *9*, 4495.

(84) Ruhman, S.; Hou, B.; Friedman, N.; Ottolenghi, M.; Sheves, M. *J. Am. Chem. Soc.* **2002**, *124*, 8854.

(85) Henderson, R.; Baldwin, J. M.; Ceska, T. A.; Zemlin, F.; Beckmann, E.; Downing, K. H. *J. Mol. Biol.* **1990**, *213*, 899.